Single Aperture Imaging Astrometry with a Diffracting Pupil: Application to Exoplanet Mass Measurement with a small Coronagraphic Space Telescope

Olivier Guyon[a], Michael Shao[b], Stuart Shaklan[b], Marie Levine[b], Mark Ammons[a], Eduardo Bendek[a], Robert Woodruff[c], Bijan Nemati[b], Joe Pitman[d]
[a]Steward Observatory, University of Arizona, 933 Cherry Ave., Tucson, AZ 85721
[b]NASA Jet Propulsion Laboratory, 4800 Oak Grove Drive, Pasadena, CA 91109
[c]Lockheed Martin Corporation
[d]Exploration Sciences, PO box 24, Pine, CO 80470

ABSTRACT

High precision astrometry of nearby bright stars is theoretically (in the photon noise limit) possible with a space coronagraph using a wide field diffraction limited camera imaging an annulus of background stars around the central coronagraphic field. With the sub-micro arcsecond accuracy theoretically achievable on a 1.4-m telescope, the mass of all planets that can be imaged by the coronagraph would be estimated. Simultaneous imaging and astrometric measurements would reduce the number of astrometric measurements necessary for mass determination, and reduce confusion between multiple planets and possible exozodiacal clouds in the coronagraphic image. While scientifically attractive, this measurement is technically very challenging, and must overcome astrometric distortions, which, in conventional telescopes, are several orders of magnitude above the photon noise limit. In this paper, we propose a new approach to calibrating astrometric distortions in the wide field imaging camera. The astrometric measurement is performed by simultaneously imaging background stars and diffraction spikes from the much brighter coronagraphic target on the same focal plane array. The diffraction spikes are generated by a series of small dark spots on the primary mirror to reduce sensitivity to optical and mechanical distortions. Small scale distortions and detector errors are averaged down to sub-micro arcsecond by rolling the telescope around the line of sight. A preliminary error budget is shown and discussed to identify major sources of error for a 1.4-m telescope imaging a 0.25 squaredeg field of view at the galactic pole.
Keywords: Exoplanets, Astrometry, Coronagraphy

1. INTRODUCTION

Detection and characterization of potentially habitable Earth-mass exoplanets is one of the leading astronomical challenges of our age. Two approaches -- direct planet imaging and host star astrometry -- have the potential for revolutionary discoveries[1]:

- Direct imaging of exoplanets with future space telescopes will reveal their atmospheric composition and possibly identify signs of biological activity.
- The precise measurement of the host star position on the sky using astrometry will yield the planet mass.

While either technique is suitable to identify new planets, both are required for unambiguous characterization of potentially habitable worlds. It has been so far assumed that coronagraphic imaging/spectroscopic measurement and mass determination require two separate missions. An approach is proposed here that combines the two critical techniques using a single space telescope in which light is simultaneously fed to a narrow field coronagraph for direct imaging and spectroscopy and a wide field astrometric imaging camera imaging a wide annulus around the central field for mass measurement with astrometry. The technique is discussed here for a medium-sized (1 to 2-m) space telescope, but could be applied on larger or smaller telescopes.

Astrometric detection of Earth-mass planets requires sub-micro-arcsecond accuracy, which is theoretically possible with a medium-size telescope imaging background stars around the bright host star. In the photon noise limit, the combined brightness of background stars in a 0.25 square degree field is sufficient to provide 1/20 of a micro-arcsecond astrometric accuracy in a 2-day observation with a 1.4-m diameter visible space telescope. The measurement is however technically challenging, and must overcome distortions which are several orders of magnitude above the photon noise limit. To address this issue, we propose to measure the astrometric motion of the host star by comparing the motion of its internally generated diffraction spikes to the background stars. The diffraction spikes are generated using a 2-D grid of regularly spaced small dark spots added to the surface of the primary mirror that do not contribute to scattered light in the central coronagraph field. Because the diffraction spikes are created on the primary mirror and imaged on the same focal plane detector as the background stars, astrometric distortions due to optics or focal plane array geometry affect equally the diffraction spikes and the background stars, and can therefore be calibrated.

2. PRINCIPLE

2.1 Overview

As shown in Figure 1, the proposed technique uses a wide field diffraction-limited imaging telescope. The central portion of the field is used for coronagraphy and reflected into a coronagraph instrument by a small pickoff mirror. The rest of the field is imaged by a wide field diffraction-limited camera which uses faint background stars as an astrometric reference. By putting dots on the primary mirror, diffraction spikes are created in the wide field astrometric image to provide a suitable reference (linked to the central star) against which the position of the background stars is accurately measured.

Since all astrometric distortions (due for example to changes in optics shapes of M2, M3, and deformations of the focal plane array) are common to the spikes and the background stars, the astrometric measurement is largely immune to large scale astrometric distortions. This concept does not require the ~pm level stability on the optics over yrs which would otherwise be essential in a wide field astrometric imaging telescope. The wide field off-axis 1.4-m diameter telescope design shown in Figure 1 produces a 0.5 deg x 0.5 deg diffraction-limited wide field image for astrometric measurement and feeds a coronagraph instrument with a 6" field of view extracted in the intermediate focus. This design is inspired from the PECO[2,3] mission concept study, and is adopted in this paper.

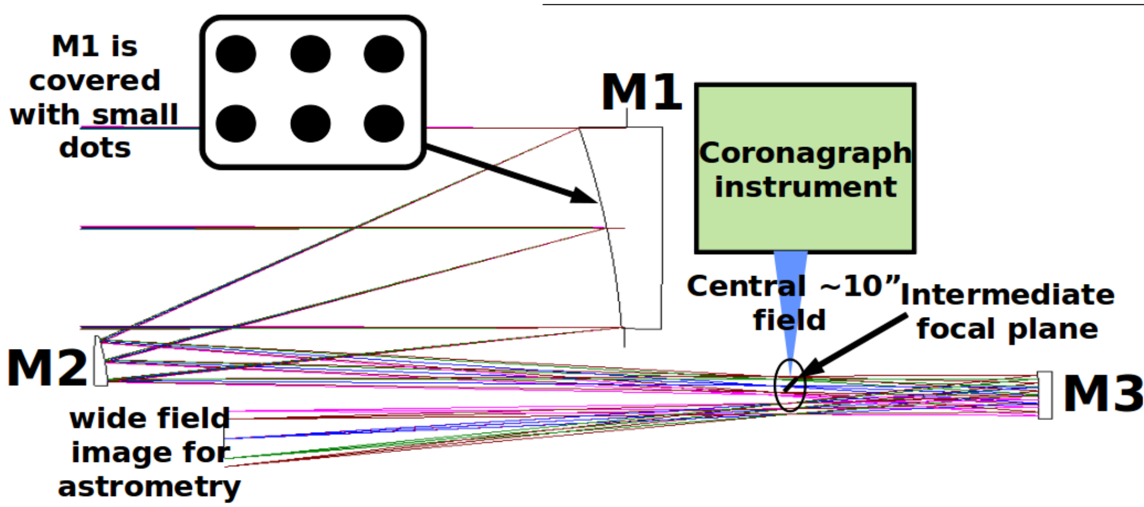

Figure 1: Example of a telescope architecture for simultaneous coronagraphic imaging and astrometry. The design shown in this figure is for a 1.4-m telescope, and offers less than 10-nm wavefront error in a 0.4 deg diameter field. The telescope primary mirror is covered with small dots.

2.2 Dots on primary mirror, spikes in the wide field astrometric camera

As shown in Figure 2, a grid of dark (non-reflective) spots is physically etched/engraved on the primary mirror. The dots act as a 2-D diffraction grating, and create a set of speckles at large angular separation from the optical axis. These speckles are radially elongated into diffraction spikes by the λ scaling factor in the focal plane. When the telescope is pointed at a bright star, these spikes will be superimposed on a background of numerous faint stars used as the astrometric reference. Precise measurement of the position of the bright central star against this background reference is possible by simultaneously imaging on a diffraction limited wide field camera both the spikes and the background of faint reference stars.

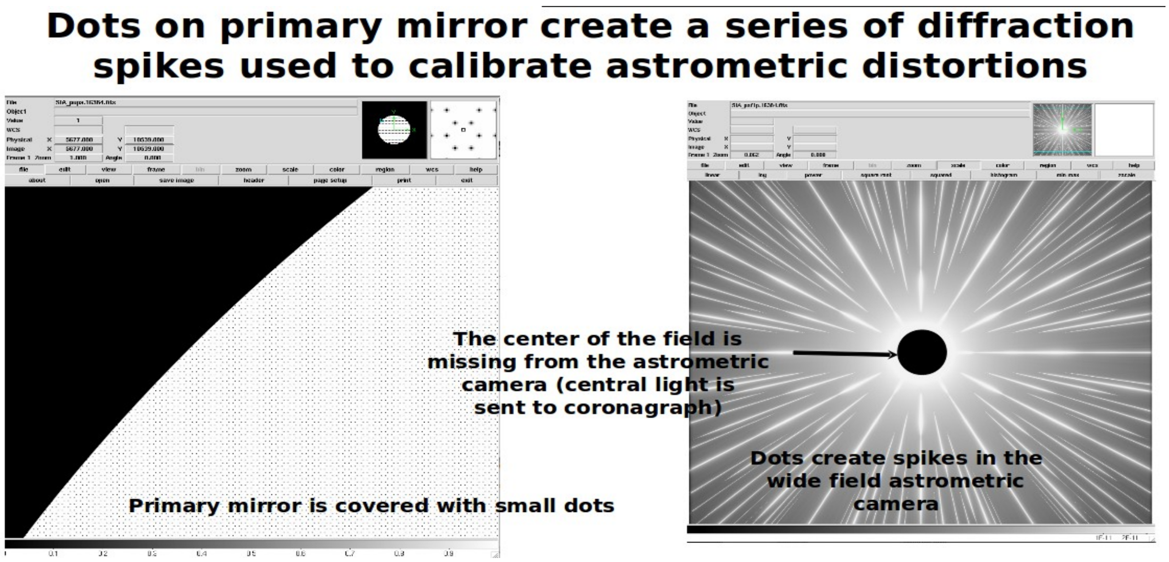

Figure 2: Dots on the telescope primary mirror (left) and corresponding on-axis PSF in the wide field astrometric camera (right).

The regular grid of small non-reflective lithographed dots covers a few percent of the surface and is deposited on the front of the primary mirror. The image at the detector is the convolution of the field distribution with the Point Spread Function (PSF) obtained by Fourier transform of the pupil function. Since the Fourier transform of a regular grid of tightly spaced dots is a regular grid of widely spaced points, the monochromatic system PSF is an Airy pattern surrounded by a widely spaced grid of fainter Airy patterns. In polychromatic light, the secondary Airy patterns are radially dispersed, producing long diffraction spikes. This PSF appears at the focal plane for each field object displaced so it is centered where its star is imaged, respectively, modulated in brightness by the source magnitude. The spikes from the background objects are therefore very dim, while the spikes from the host star are much brighter. Light in the central part of the field is directed to the coronagraph, therefore suppressing its bright central Airy pattern while passing its polychromatic diffraction pattern (aka spikes) to the focal plane array used for astrometry.

The dots serve two purposes:

- **Provide an adequately bright signal for the host star light.** The host star is much brighter than the background stars used for astrometry. By distributing a few percent of the host star's light over a large number of pixels, the spikes provide a feature that can be imaged without saturation on the same detector as the background stars. A similar magnitude compensation scheme using a grating in front of the telescope has previously been used over small angles for ground-based astrometry of binary stars[4], and more recently with a grating in a relay pupil for coronagraphic imaging and astrometry of faint companions with adaptive optics[5,6]. A related technique is also being used at the NASA Ames coronagraph testbed, where the location of the star and its brightness are measured by comparison with diffraction spikes generated by the periodic print-through structure on the deformable mirror.
- **Calibrate changes in astrometric distortions** between different observations of the same target. Optical distortions due to changes in the shape and alignment of the telescope optics and physical distortions of the focal plane detector array create astrometric measurement errors. These distortions move the spikes and the background stars by the same amount. Careful comparison of spikes images acquired at two epochs is used to map astrometric error changes. Instead of directly measuring the position of the background stars relative to the host star, this concept measures locally how the background stars move relative to the spikes around them. Since the dots are placed directly on the primary mirror, which acts as the system's entrance pupil, all distortions are common to the spikes and the background stars, including telescope pointing errors. If the grid of dots were placed after in a relay pupil (as done in some ground-based telescopes), astrometric distortions upstream of the grid would not be calibrated, and micro arcsecond accuracy astrometry would require picometer

stability of the telescope optics ahead of the dotted mask. A more detailed description of this effect is provided in section 2.3.

2.3 Immunity to field distortions

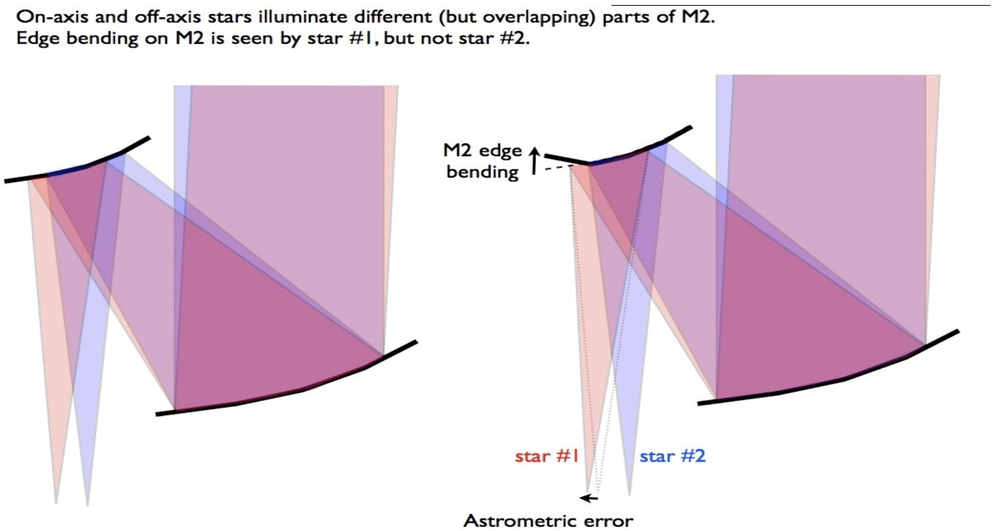

Figure 3: Tilt anisoplanatism due to changes in M2's shape creates an astrometric error.

Astrometry with conventional telescopes is hampered by astrometric distortions introduced by the optics and the atmosphere. Any wavefront error introduced ahead or after the telescope's pupil plane creates variations in the plate scale in the focal plane. This effect is known as tilt anisoplanatism, and is the main limitation to precision astrometry on ground-based telescopes[7]. In space, with no atmosphere, astrometric distortions are much smaller, but still exist due to bending in optics within the telescope and instrument. Figure 3 shows how changes in the telescope's secondary mirror shape produce an astrometric error.

The proposed scheme eliminates this problem since the reference pattern (diffraction spikes) is introduced directly on the primary mirror (PM) of the telescope. The dots on the PM act as a diffraction grating creating secondary beams which emerge from the primary mirror with slightly different angles and travel through the optical system up to the focal plane. Light from an off-axis star and light from a nearby diffraction spike go through the same path in the optical system (telescope + instrument) and share the same astrometric distortion. The the anisoplanatism problem is therefore eliminated in the differential spike/backround star astrometric measurement . The proposed scheme is also insensitive to focal plane array distortions, as they will affect equally the background stars and the diffraction spikes. Wavefront errors on the primary mirror do not produce an astrometric error as they are common to both the diffracted beams and the beam from the astrometric reference stars.

For the spikes to encode the same astrometric distortions as the background stars:

- **The dots must cover uniformly the primary mirror**, otherwise, changes in PM shape can create a differential motion between the spikes and the background stars. For example, if the dots cover only a zone of the PM, the spikes will move with the average wavefront slope over the area of the PM covered with dots, while background stars will move with the overall wavefront slope over the whole PM.
- **The primary mirror must the aperture stop for the system**.
- **There must not be any refractive optics between the primary mirror and the wide field camera detector**. Refractive optics have some chromaticity, and the spikes are chromatically elongated (a background star and a spike near it therefore have very different colors, and could see different distortions in a system with refractive optics).

The design studied in this document fullfills these 3 requirements.

2.4 Simultaneous operation with a coronagraph

Since the primary mirror mask is a regular grid containing no low order aberrations, it does not impact high contrast coronagraph observation performed by a separate narrow field instrument, other than a small loss in throughput: as seen by the coronagraph, the pupil is uniformly grey, with a few percent of the light missing (equivalent to a uniform loss in reflectivity in the coating). The astrometric measurement is a good match to an internal coronagraph:

- Internal coronagraphs use highly stable telescopes providing stable PSFs and a thermally stable environment for the wide field camera. This will help with the astrometric measurement accuracy.
- Coronagraphs observe a small number of bright targets with long exposure times and with several revisits - this observation mode is also suitable for the astrometric measurement.

3. DATA ACQUISITION AND PROCESSING

3.1 Measurement and astrometric distortion compensation

The astrometric signal to be measured is a 2-D translation of the foreground star against a set of fainter background stars used as the astrometric reference. As shown in Figure 4, the telescope is pointed on the central star, so the spikes, in principle, do not move between observations, but the background stars move on the detector due to the astrometric motion of the central star (vector in Figure 4, left panel). The telescope pointing is essentially dragged by the motion of the foreground star over the course of the mission (several years). The vector in the left panel of Figure 4 is what the instrument measures as a function of time. This vector is the sum of the foreground star proper motion, the parallax motion and the astrometric signal imprinted by one or several planets. The measurement needs to be repeated at several epochs (typically 10 or more) to unambiguously separate these terms and measure the planet's orbit and mass.

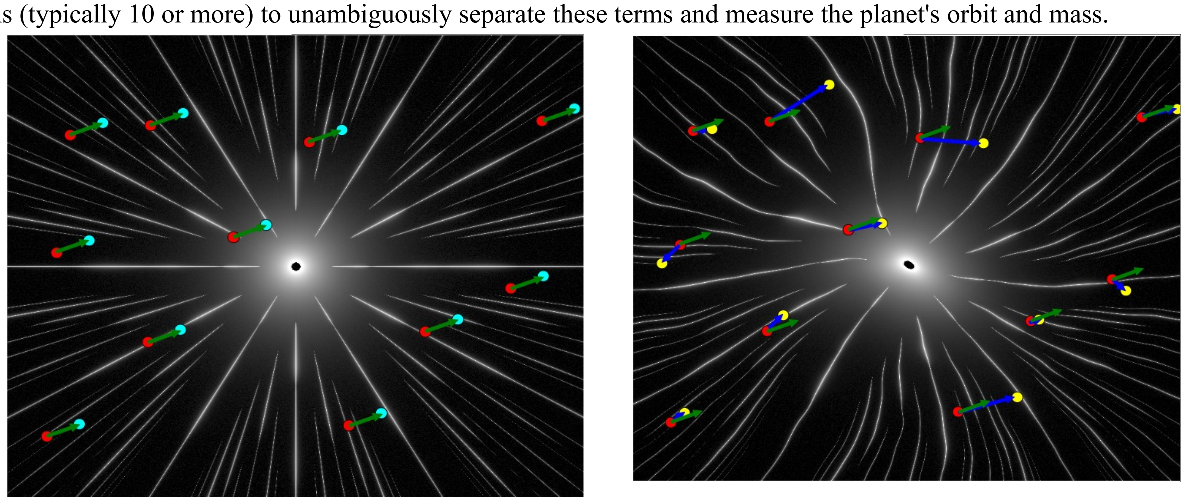

Figure 4: Measurement principle. (left) A set of background stars is imaged in a wide field of view around the central star. The positions of the background stars is shown in this figure for two observation epochs. The vector (to be measured) is the astrometric motion of the central star between the 2 observations. The motion of the background stars has been greatly exagerated in this figure to illustrate the measurement. (right) Effect of astrometric distortions on the image. Due to astrometic distortions between the 2 observations, the actual positions measured are different from the points at the end of the vectors on the left panel. With a wide field camera, the error is much larger than the signal induced by a planet, which makes the astrometric measurement impossible without distortion calibration. For illustrative purpose, the distortion shown here is 1e6 times larger than expected from high quality optics in the 1.4-m TMA design considered in this study.

Instrumental astrometric distortions are due to non-ideal optics shapes and detector geometry. While most of the distortions are expected to be static, some are dynamic (variable between observation epochs). Over a fraction of a degree, the instrumental distortions are much larger than the astrometric signature of a planet. As shown in Figure 4, the distortions affect both the background stars and the diffraction spikes, so the diffraction spikes can be used to calibrate them. The measured astrometric motion (blue vectors in Figure 4) is the sum of the true astrometric signal (green vectors) and the astrometric distortion induced by changes in optics and detector geometry between the two observations. Direct comparison of the spike images between the two epochs is used to measure this distortion, which is then subtracted from the measurement to produce a calibrated astrometric measurement.

The calibration of astrometric distortions with the spikes is only accurate in the direction perpendicular to the spikes length: with finite SNR, it is practically impossible to detect a radial motion of the spikes (note: spectral features introduced by a filter could in principle remove this limitation at the expense of throughput). For a single background star, the high precision measurement is therefore made along the axis perpendicular to the spikes (1-D measurement). The 2-D measurement is obtained by combining all 1-D measurements.

3.2 Telescope roll

Detector imperfections can have a large effect on astrometric accuracy. There are two approaches to mitigate this problem:

- Keep the star(s) on nearly the same pixel position between measurements to perform a differential measurement which is insensitive to detector imperfections, or
- Average down detector defects by performing a large number of measurements over different pixels.

The first approach is not possible: it is not possible to keep background stars on exactly the same pixels of the detector during the measurement timescale (several yr between the first and last measurement) due to proper motion, parallax motion and the aberration of light. Since background stars cannot be kept on the same pixels, each measurement of the motion of a background star between two epochs compares PSFs falling on different pixels with different characteristics (pixel sensitivity, size, shape etc..). Many statistically independent measurements are required to average this error term. This averaging is achieved by both combining the position measurements of a large number of background stars and rolling the telescope along the line of sight to move the background stars' PSFs over a large number of pixels. The roll geometry is shown in Figure 5.

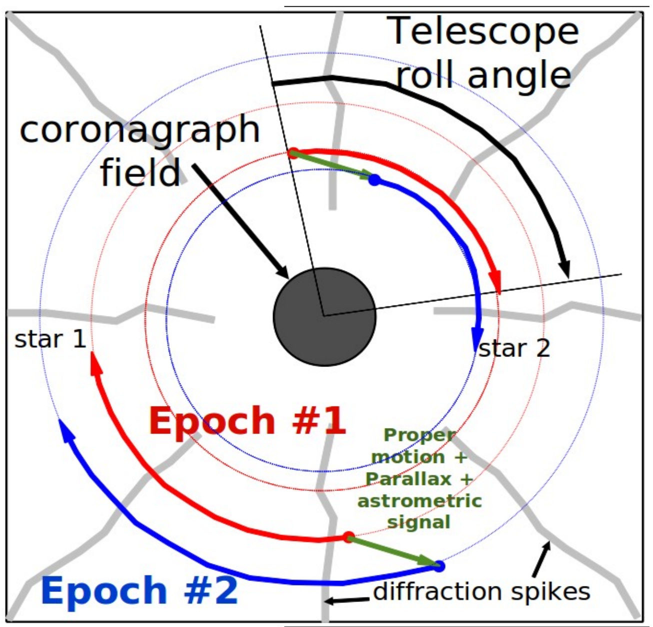

Figure 5: Position of two background stars on the camera focal plane during telescope roll. Observations at two epochs (colored red and blue) are shown for the two stars.

The telescope roll is very efficient at reducing the contribution of detector errors to the final astrometric measurement. During a single observation (typically a day), the telescope is slowly rolled around the line of sight to move the background PSFs on the focal plane. On a large format detector, a roll angle of a few tens of degrees is large enough to move the PSF by several thousand pixels, and a 1 radian roll will produce about 10000 PSF centroid measurements per star.

Unknown flat field errors produce astrometry measurement error: a pixel which is more sensitive than assumed will attract the measured position while pixels less sensitive that assumed will push away the measured position. Figure 6 shows how this measurement error (red arrows) evolves as the PSF drifts across the detector during telescope roll. The error can be decomposed into a radial component (along the direction to the central star) and a longitudinal component. When integrated over time, the residual error is almost entirely radial, as the longitudinal error when the PSF approaches the defective pixel is compensated by the opposite error when the PSF drifts away from the defective pixel. The telescope roll can therefore almost entirely remove flat field induced errors along the axis where the astrometric measurement is performed.

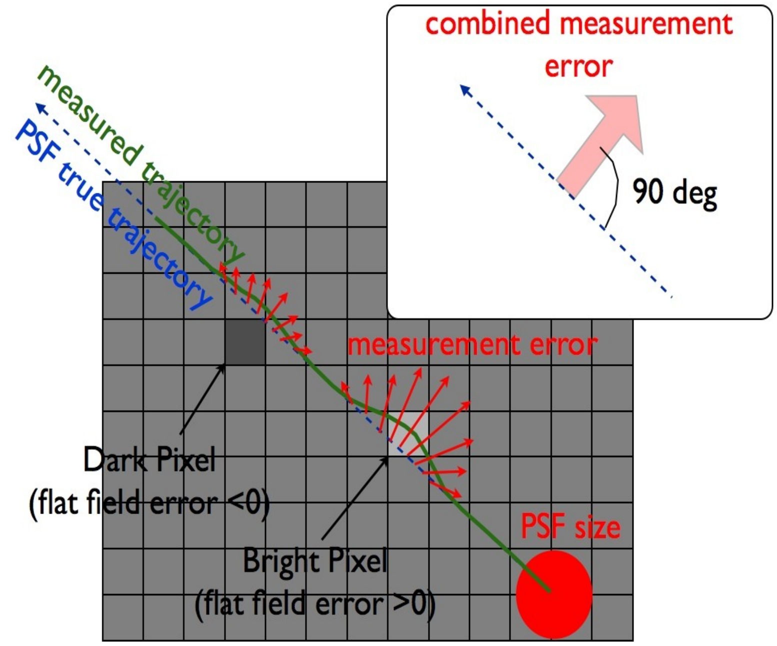

Figure 6: Effect of flat field errors between pixels on the astrometric measurement of a PSF moving in a straight line. The true PSF trajectory (blue) differs from the measured PSF position (green curve) due to the presence of "bright" and "dark" pixels. When compensated for the telescope roll, the combined measurement error is perpendicular to the PSF motion: there is no error along the direction of the PSF motion.

The discussion above assumes sensitivity differences between pixels, but is also valid for other differences between pixels, such as a pixel with a peculiar color "preferences", or a pixel with a "dead corner". The key advantage of the roll is that it transforms detector defect induced astrometric errors into a time-variable error which is strongly anticorrelated on both sides of the defect. These errors therefore disappear in the averaged measurement (this is much better than a decorrelated error which slowly decreases as 1/sqrt(T)).

3.3 Data processing overview

The data acquired is represented in the top left part of Figure 7. The astrometric measurement is performed differentially, between sets of images acquired at 2 epochs. The top row shows 4 images acquired at epoch 1. The telescope is rolled between each image: the diffraction spikes are fixed on the detector but the background stars (grey spots labeled 1, 2 and 3 in the top left image of the figure) rotate around the line of sight. The same sequence of measurements is repeated at epoch 2 (second row). The displacement of the background stars compared to the central star (and the spikes) is shown as red arrows in the epoch 2 images. The background stars are located almost (but not exactly) on the same position on the detector at the two epochs. This configuration is largely immune to uncalibrated/unknown PSF shape, as the PSF is not expected to change sufficiently over a sub-arcsec field to introduce an astrometric error. Maintaining nearly the same PSF positions between epochs also greatly reduced sensitivity to large static distortions (which should also be removed by the spike calibration). The position of the star on the detector is measured by fitting a model of the PSF on a model of the pixel geometry and sensitivity map (including sensitivity variations within the pixels, if known). The position offset $(dx_{i,j},dy_{i,j})$, the difference between background star position at two epochs, is measured for each star i in the field for each roll angle position j.

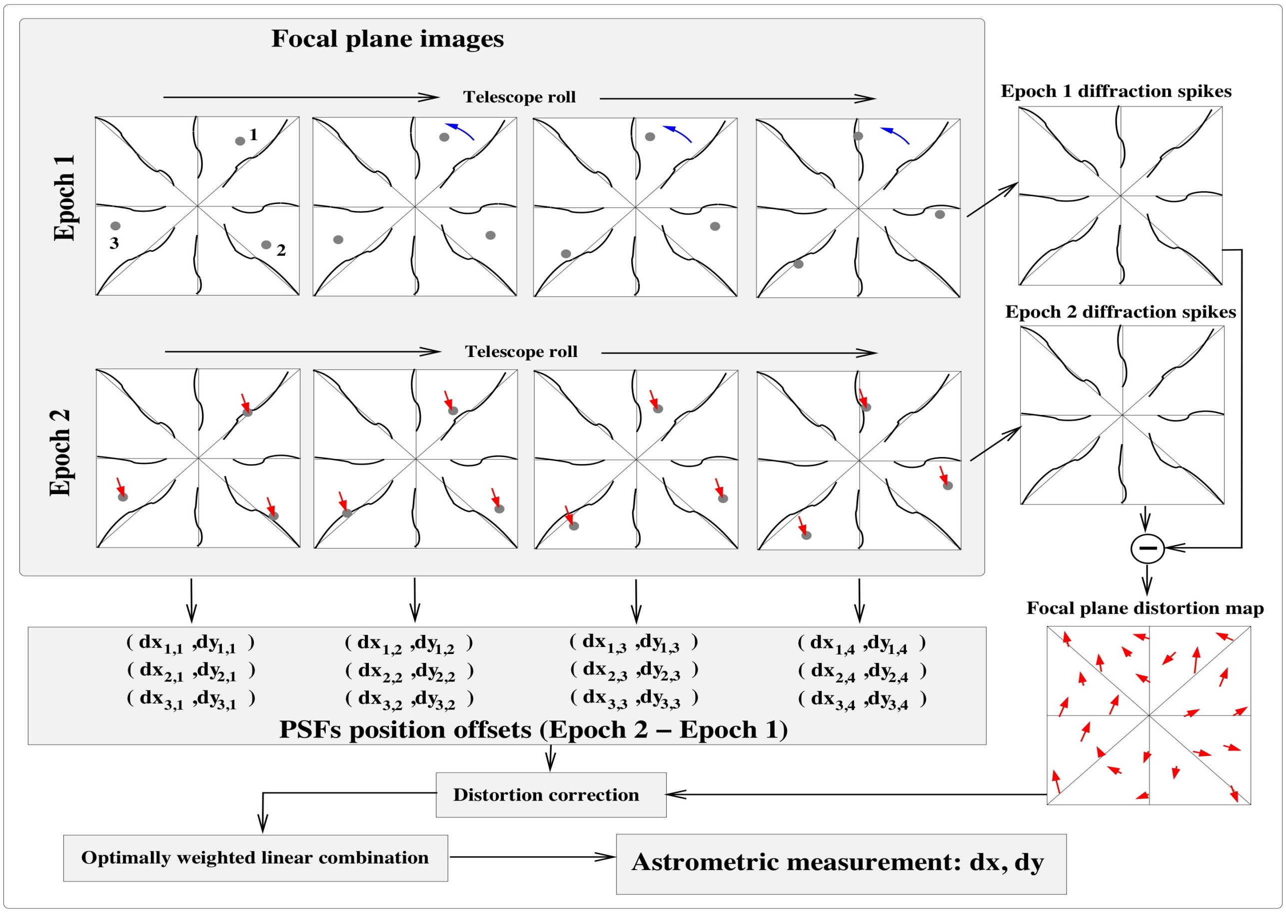

Figure 7: Data acquisition and data processing overview.

The diffraction spikes are kept at approximately the same position on the detector for all observations, and possible time-variable field distortions are measured by small changes in the shape/location of the spikes. These distortions are only measured along the spikes and a 2-D interpolation is used to build a continuous 2-D map of the distortion change between the two epochs. This distortion map is removed from the measurements. The final 2-D astrometric measurement is obtained by combining all 1-D measurements with appropriate weighting coefficients (fainter stars where the photon noise contribution is large are given a smaller weight).

4. SCIENCE GOALS AND PERFORMANCE

It is assumed that a 1.4-m telescope is used with a coronagraph offering a 2 λ/D inner working angle, modeled after the PECO mission concept.

4.1. Primary Science Goals

The science goals of the astrometric camera are twofold:

- Assist the coronagraph to **detect exoplanets**. At the minimum, the astrometric measurement should confirm detections performed by the coronagraph and help constrain their orbital parameters.
- **Measure the mass** of all planets imaged by the coronagraph in the habitable zone of nearby stars

The second goal (mass measurement) is the most challenging. The PECO coronagraph system is adopted in this study. In this section, we estimate what astrometric measurement accuracy is required to achieve these goals. The mass estimation accuracy is function of planet type, stellar brightness (bright stars are easier, as their spikes are brighter in the astrometric camera) and star distance (stars further away produce a smaller astrometric signal). The most challenging planets to be detected by PECO are Earth-like planets. Super-Earth and giant planets are easier to observe, both for the coronagraph and the astrometric camera. The faintest star in the list of the six PECO targets for Earth-like planets imaging is m_V = 3.7, and the most distant stars are at distances of 6.0, 6.1 and 7.5 pc. A Sun analog at 6 pc from Earth is therefore a representative example of a challenging target for the coronagraph. Its apparent magnitude is m_V=3.7, equal to the faintest target for which PECO coronagraph can detect a Earth analog.

An Earth Mass planet is placed at 1.2 AU around this star (to avoid the 1 yr period blind spot with the astrometric measurement). For this target, the astrometric accuracy required to measure the planetary mass to 10% relative accuracy is derived in this section, and adopted as a requirement for the astrometric instrument. **The astrometric instrument is therefore designed to measure the mass of all targets imaged by the PECO coronagraph to 10% relative accuracy or better.**

4.2. Measurement scheme

The planet orbit and mass are simultaneously measured by combining the astrometric and coronagraphic data, as illustrated in figure 8.

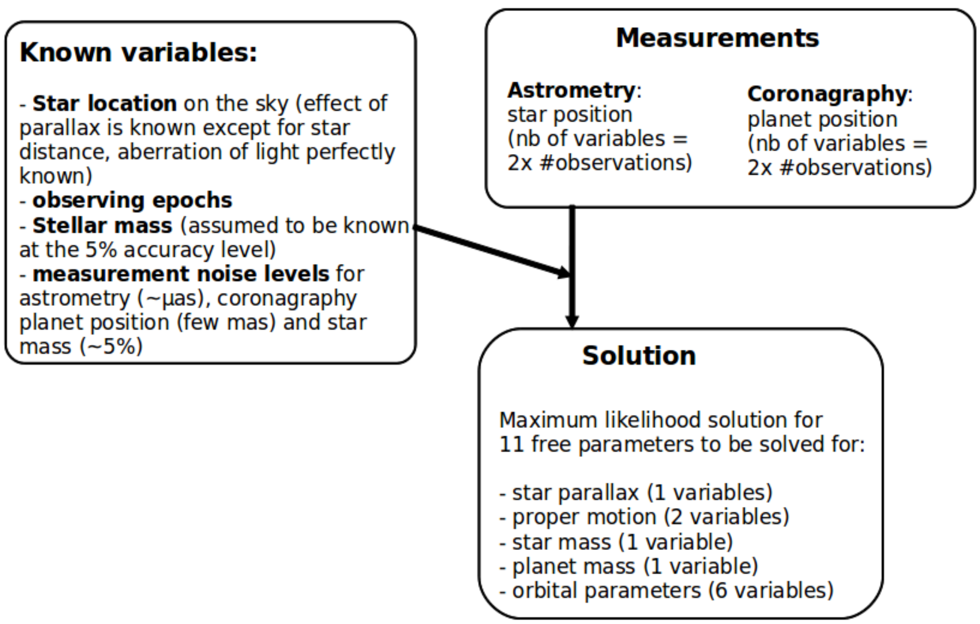

Figure 8: Combined astrometry and coronagraphy measurement principle. The planet orbital parameters and mass are estimated by fitting both the astrometry and coronagraphy data.

4.3 Required astrometric measurement accuracy

The 1-D measurement accuracy is defined here as the standard deviation of a series of a series of 32 1-D astrometric measurement after parallax and proper motion have been fitted and removed from the 2-D astrometric measurements. To estimate the astrometric measurement accuracy required to meet science requirements, simultaneous coronagraphic and astrometric measurements were simulated and fitted according to the scheme shown in Figure 8. Figure 9 shows the planetary system architecture and geometry used for the simulation. Results of the simulation are compiled in figure 10, which shows how the planet mass estimate changes as a function of the level of astrometric error per measurement. Figure 10 shows that a 10% relative precision in the estimate of the Earth-mass planet requires a 0.2 µas accuracy per astrometric measurement.

Planetary system characteristics	
Star	Sun analog
Distance	6 pc
Location	Ecliptic pole
Orbit semi-major axis	1.2 AU
Planet mass	1 Earth mass
Orbit excentricity	0.2
Astrometric signal amplitude	0.5 µas
Orbit apparent semi-major axis	200 mas
Observations	
Number of observations	32 (regularly spaced every 57 days)
Coronagraph: planet position measurement accuracy in coronagraphic image	2.5 mas per axis (= 3.6 mas in 2D): corresponds to diffraction-limited measurement with 100 photon at 550 nm on PECO
Coronagraph: Inner Working Angle	130 mas (coronagraph cannot see planet inside IWA)
Astrometry: accuracy	Variable (to be matched to science requirements)

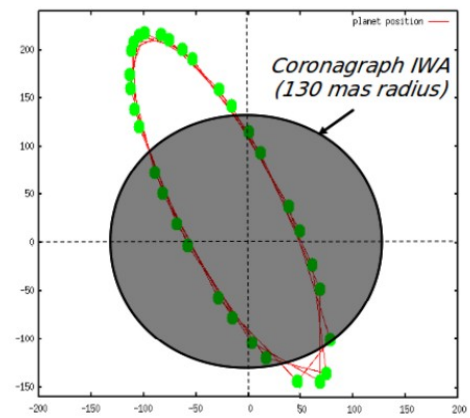

Figure 9: Simulation parameters (left) and planet orbit geometry in the coronagraph (right). The planet is outside the coronagraph IWA for 17 out of the 32 observations.

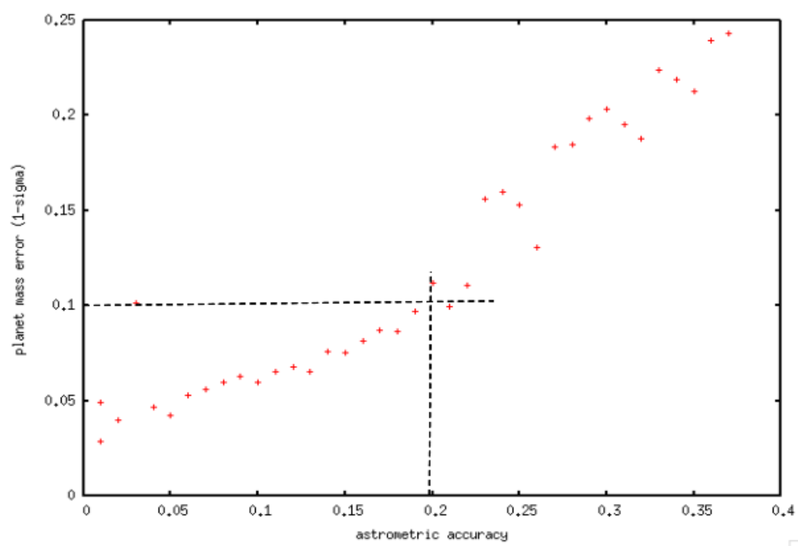

Figure 10: Mass measurement error as a function of astrometric single measurement accuracy. To reach a 0.1 M_{Earth} estimation error, the single measurement, single axis astrometric accuracy needs to be 0.2 µas.

4.4 Science benefits of simultaneous coronagraphic imaging and astrometric measurement

Coronagraph images provide an accurate measurement of the orbital parameters (more precise that astrometry), but no mass measurement. For a 1 M_{Earth} planet on a 200mas radius orbit around a Sun-like star, a 2.5 mas position measurement accuracy in the coronagraphic image (~1/20 λ/D in the blue for a 1.4-m telescope) corresponds to 1/80 of the orbit radius, which is equivalent to a 0.007 µas astrometric precision. As illustrated in Figure 11, solving for planet mass using the combined astrometry + coronagraphy measurements is therefore very powerful, and allows more accurate mass determination than would be possible with astrometry alone:

- The coronagraphic images contraint the orbital parameters and reduce error propagation from orbital parameter to mass estimate
- With both coronagraphic imaging and astrometry, the star mass is directly measured. The planet mass is therefore also directly measured (astrometry alone would only measure the planet to star mass ratio)

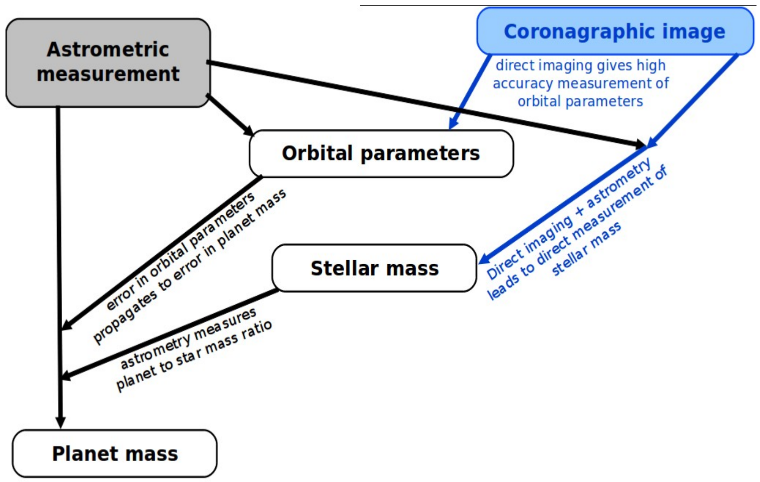

Figure 11: The complementarity between coronagraphic and astrometric measurements allows a better planet mass estimate than would be possible with astrometry alone.

The standard deviation for all parameters of the fit is shown in table 1, for both astrometry only and astrometry + coronagraphy. With coronagraphic images, the standard deviation on orbital parameters is reduced by approximately a factor 10, and the stellar mass is directly measured, while with astrometry only, it is assumed with a 5% standard deviation. The planet mass is estimated with a standard deviation below 0.1 M_{Earth} with the combined data, while it would be 13% larger with astrometry only.

Table 1: Comparison between astrometry alone and astrometry + coronagraphy: standard deviation for fit parameters

	Standard deviation	
	Astrometry only	**Astrometry + coronagraphy**
parallax	0.037 µas	0.035 µas
x proper motion	0.017 µas/yr	0.012 µas/yr
y proper motion	0.020 µas/yr	0.013 µas/yr
Planet mass	0.132 M_{Earth}	0.098 M_{Earth}
Semi-major axis	0.0228 AU	0.0052 AU
orbital phase	0.653 rad	0.039 rad
orbit inclination	0.0968 rad	0.0065 rad
sma projected PA on sky	0.1110 rad	0.0040 rad
orbit ellipticity	0.098	0.0035
PA of perihelion on orbit plane (w)	0.648 rad	0.0034 rad
stellar mass	0.050 M_{Sun}	0.013 M_{Sun}

Mitigating the 1-yr period astrometric blind spot: The astrometric signature of a planet in a one year period orbit is absorbed in the parallax fitting of the astrometry measurements. With astrometric measurements only, the mass estimate error therefore grows as the planet period becomes closer to 1yr. The width of this blind spot is reduced as the astrometric measurements span a longer period of time. To illustrate how coronagraphic images mitigate the astrometric blind spot problem, we consider here a 1 Earth mass planet at 1.01 AU from a Sun mass star (period = 1.015 yr) at the ecliptic pole, orbiting a star at 6pc. We assume circular orbits (for both the Earth and the target planet), and a planet orbit phase equal to Earth orbit phase plus 1 radian, with a face-on orbit. The system is observed 32 times over 5 yr with observations regularly spaced in time. We assume that the astrometric measurements have a 0.3 μas single axis accuracy, and that the images allow measurement of the planet position to 5 mas per axis (unless the planet is within the 130 mas IWA of the coronagraph). With astrometry only, the planet is not detected: its mass is estimated at 3.25 M_{Earth} with a 4.17 M_{Earth} standard deviation. With astrometry and coronagraphic imaging, the planet is detected and it mass estimated to be 1.01 M_{Earth} with a 0.16 M_{Earth} standard deviation.

Broader benefits of a combined astrometry and coronagraphy measurement. Other benefits of performing astrometry and coronagraphy simultaneously include:

- Reduces confusion with multiple planets. Outer massive planets (curve in the astrometric measurement) will be seen by the coronagraph
- Astrometry will separate planets from exozodi clumps
- Astrometric knowledge allows to extract fainter planets from the images, especially close to IWA, where the coronagraph detections are marginal

5. ERROR BUDGET AND NUMERICAL SIMULATIONS

5.1 Error Budget Overview

Error terms are listed in table 2, and can be grouped in 4 categories:

- Astrophysical noise: Includes stellar activity on the central star[8] and astrometric wobble of background reference stars.
- Fundamental measurement noise: Measurement noise due to the primary design parameters such as telescope diameter, pixel sampling and wavelength. This would be equal to the total instrument noise in the absence of defects in the detector or optical train. Includes photon noise contribution from background stars and zodi background.
- Static astrometric error terms: Contribution of all static defects, such as poorly calibrated detector response or manufacturing errors in the optical surfaces. Even perfectly static defects produce astrometric errors, as the trajectories of the background stars on the focal plane are slightly different between observations (proper motion, parallax).
- Dynamic astrometric error terms: Errors due to changes of the telescope and instrument between observations. Includes variations in the shape of optics surfaces, variations in detector geometry (detector pixels move between observations) and variations in detector sensitivity. Dynamic errors are not fully calibrated by the spikes (spikes have a limited SNR, and do not fully sample the field of view). Dynamic errors can also create errors in the measurement of the spikes positions.

Table 2: Overview of main error budget terms. Error budget terms are divided in 4 categories: astrophysical noise, fundamental measurement noise, static astrometric error terms, and dynamic astrometric error terms.

Noise term	Description	Impact
Sunspots and stellar activity	The central star photocenter moves due to stellar activity and sunspots, creating an astrometric signal	Small to moderate
Astrometric signal of background reference stars.	Several background stars have astrometric motions due to multiplicity and planets	Small thanks to large number of background stars (averaging). Background stars are also distant and low metallicity (Halo stars)
Photon noise on background stars	Photon noise limits the position measurement accuracy on faint stars. The faintest stars are below the zodiacal light level.	Dominant on faint stars
Photon noise due to zodiacal light		
Detector finite sampling of a polychromatic PSF	The position measurement error is somewhat larger than the photon-noise limit.	Small for Nyquist sampled image
Detector readout noise		Small if exposure time is properly chosen

Detector flat field, and sensitivity variations within pixels	These unknown errors produce errors in the position measurement of background stars. Thanks to their roll anticorrelation, they average down quickly with roll.	Small thanks to roll averaging
Static astrometric distortion due to optics surface figure	Between observations, the trajectory of background stars moves slightly on the focal plane due to proper motion and parallax of the central star. This transforms static distortions into a small time-variable astrometric error.	Moderate to strong Can be mitigated by increasing total light in spikes, which allow (1) smaller spacing between spikes in focal plane, and (2) reduced impact of spike photon noise on the astrometric calibration
Static astrometric distortion due to unknown detector geometry		
Dynamic astrometric distortion due to change in optics surface figure	Mirror shapes change between observations, and this distortion is not perfectly removed by the astrometric calibration using diffraction spikes	
Dynamic astrometric distortion due to change in detector geometry	The large focal plane array is likely made of many individual chips which can move and deform. This distortion is not perfectly removed by the astrometric calibration using diffraction spikes.	
Dynamic astrometric distorition due to change in detector response	Unknown changes in detector response are misidentified as a motion of the spikes, creating a change in the astrometric calibration	Significant if > 1%
Dynamic astrometric distorition due to spots moving on mirror	Spots move on the PM between observations, creating a differential motion between spikes and background stars	Small ?

5.2 Numerical simulations: goals and approach

A numerical simulation was developped to quantify the measurement noise terms outlined in the previous section (all noises except the astrophysical noise). The astrometric distortions in the system are computed with 3D raytracing (code written in C, agreement with Code V has been verified). Focal plane images are produced by Fourier transform, and then distorted according to geometrical optics. Image sizes are 16k x 16k pixel. The telescope and instrument parameters used for the simulation are shown in table 2, where values are given for the main instrumental sources of measurement errors. Table 3 shows that the system simulated differs from the final system (which meets the science requirement). The difference is entirely due to computing limitations:the full scale system image sizes would be 40kx40k pixel (>6 GB per image), too large for the fast and easy computation of the astrometric measurement accuracy necessary for parameter optimization and searches (note that all simulations shown here were performed on a laptop computer, and a more powerful computer could perform the computations on a full scale system).

Table 3: Main telescope and instrument parameter values adopted for the numerical simulation.

	Value in simulations	**Value for mission**	**Rationale for flight instrument value**	**Impact on astrometric accuracy**
Telescope diameter (D)	1.4 m		PECO sized, cost constrained	Astrometric accuracy goes as D^{-2}, thanks to larger collecting area and smaller PSF size (assuming constant FOV)
Detector pixel size	44 mas		Nyquist at 600 nm	Little impact as long as sampling is close to or finer than Nyquist
Field of view (FOV)	0.03 sq deg (0.1 deg radius)	0.25 sq deg (0.5 deg X 0.5 deg)	low WF error across field, 1.6 Gpix detector	Astrometric accuracy goes as $FOV^{-0.5}$
Single measurement time	48 hr		Typical single observation	Astrometric accuracy goes as $t^{-0.5}$

			duration for coronagraph	
Dot coverage on PM (area)	1%	8%	Keeps thoughput loss moderate in coronagraph	Larger dot coverage allows observation of fainter sources.
Flat field error after calibration, static (high spatial frequency)	1.02% RMS, 6% peak		Conservative estimate for modern detector after calibration	Negligible effect on background PSF measurement (well averaged with roll)
Flat field error, dynamic	10^{-4} RMS per pixel, uncorrelated spatially and temporally between observations		10^{-4} loss in sensitivity for each pixel over 48 hrs = 2% per year = 10% over 5 yrs	Negligible effect on background PSF measurement, but significant effect on measurement of spikes locations
Telescope roll	1.0 rad (+/- 0.5 rad)		Manageable sunshielding	Larger telescope roll leads to better averaging of detector errors
Uncalibrated change in optics surface between observations for M2 & M3	40 pm		Wavefront measurement repeatability (optical element removed / reinserted) obtained when testing similar sized optics on ground	Larger change in optics surface reduces astrometric accuracy
Static optics surface errror (M3 mirror)	1.5 nm		WF error and PSD taken from similar existing optical element	Small impact on performance, as background PSFs are almost fixed between observations
Astrometric accuracy, single measurement, single axis, m_V=3.7, galactic pole	***0.58 μas***	***0.20 μas***	***0.2 μas is required to achieve science goals***	

The details of the numerical simulation tool are given in figure 12, which shows how the input parameters for the mosel are used to estimate the final astrometric accuracy. This figure is explained in more detail in a separate document[9] which is not included in this paper.

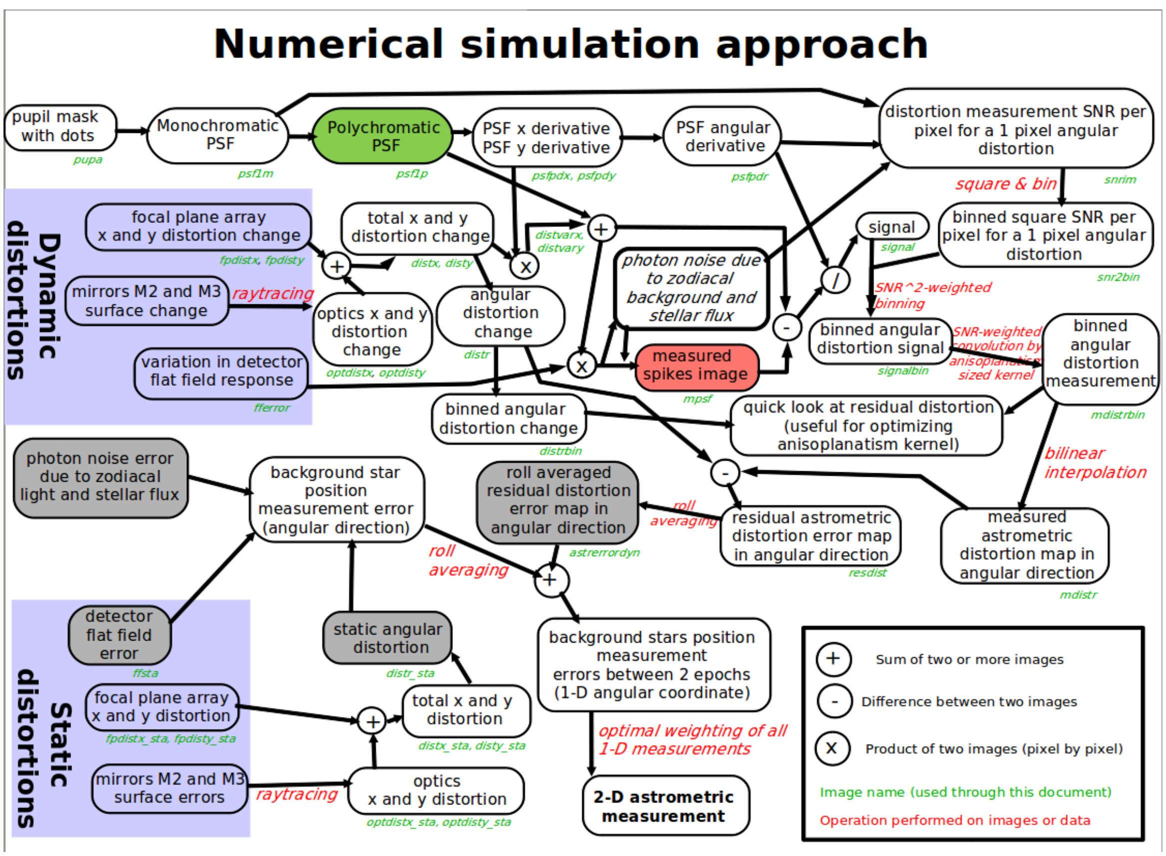

Figure 12: Numerical simulation overview.

5.3 Expected astrometric measurement accuracy

According to the numerical simulation peformed, the expected single measurement single axis astrometric measurement accuracy is 0.2 µas for the nominal 0.25 sq deg FOV / 1.4-m diameter telescope system (0.58 µas for the 0.03 sq deg simulated system). Figure 13 shows, for the 0.03 sq deg FOV system, that the astrometric measurement accuracy is independant of star brightness for stars brighter than mV=7, and that it grows for fainter stars. Using simple scaling laws, table 3 estimates the single measurement astrometric accuracy for a range of telescope diameter and field of view values.

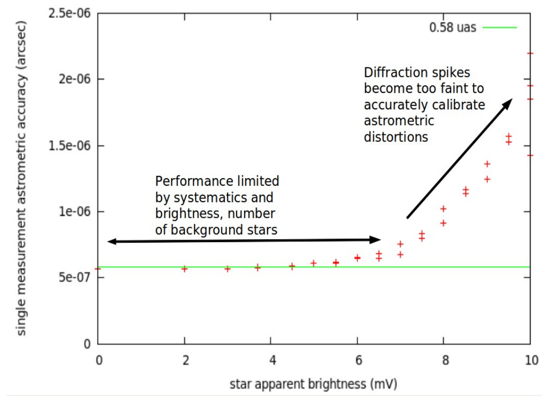

Figure 13: Single measurement, 1-D astrometric measurement accuracy as a function of star brightness for a 0.03 sq deg FOV system.

Table 3: Single measurement, 1-D astrometric measurement accuracy as a function of field of view and telescope diameter.

	FOV = 0.03 sq deg	**FOV = 0.1 sq deg**	**FOV = 0.25 sq deg**	**FOV = 0.5 sq deg**	**FOV = 1.0 sq deg**
D = 1.4 m	0.58 µas	0.31 µas	0.20 µas	0.14 µas	0.11 µas
D = 2.0 m	0.28 µas	0.15 µas	0.10 µas	0.07 µas	0.05 µas
D = 3.0 m	0.13 µas	0.067 µas	0.044 µas	0.030 µas	0.024 µas
D = 4.0 m	0.071 µas	0.038 µas	0.025 µas	0.017 µas	0.013 µas

6. CONCLUSION AND FUTURE WORK

Astrometric measurement of nearby bright stars at the sub-micro-arcsecond appear feasible with a medium-sized space telescope, and could be performed simultaneously with coronagraphic imaging. Our current model of the astrometric measurement will be improved in the near future to include a more accurate and quantitative description of the main error terms. We will also add several terms which have not yet been evaluated, including telescope alignment, defects in the spots on the PM (including small motion of the spots on the mirror), and coating degradation effects. A laboratory validation of the concept is in preparation. It will be used to verify error terms, when applicable, and develop and test data analysis algorithms.

REFERENCES

[1] Shao, M., Catanzarite, J., Pan, X., “The Synergy of Direct Imaging and Astrometry for Orbit Determination of exo-Earths”, ApJ, in press (2010)

[2] Guyon et al., PECO website: http://caao.as.arizona.edu/PECO/ (2010)

[3] Guyon et al., “The pupil mapping exoplanet coronagraphic observer (PECO)
”, SPIE paper 7731-80 (2010)

[4] Strand, K. Aa., “Photographic observations of double stars made with the 24-inch Sproul refractor”, AJ, 52, 1 (1946)

[5] Sivaramakrishnan, A., Oppenheimer, B.R., “Astrometry and Photometry with Coronagraphs”, ApJ, 647, 620 (2006)

[6] Zimmerman, N., et al., “Parallactic Motion for Companion Discovery: An M-Dwarf Orbiting Alcor”, ApJ, 709, 733-740 (2010)

[7] Cameron, P. B., Britton, M. C., Kulkarni, S. R., “Precision Astrometry With Adaptive Optics”, ApJ, 137, 83-93 (2009)

[8] Makarov, V. V., Beichman, C. A., Catanzarite, J. H., Fischer, D. A., Lebreton, J., Malbet, F., Shao, M., “Starspot Jitter in Photometry, Astrometry, and Radial Velocity Measurements”, ApJ, 707, L73-L76 (2009)

[9] Guyon et al., http://www.naoj.org/staff/guyon/04research.web/30astrometry.web/content.html (2010)